Reducing 4DCBCT Imaging Time and Dose: The First Implementation of Variable Gantry Speed 4DCBCT on a Linear Accelerator.

Ricky T O'Brien[1], Uros Stankovic[2], Jan-Jakob Sonke[2] and Paul J Keall[1]

[1]Radiation Physics Laboratory, Sydney Medical School, The University of Sydney, NSW 2006, Australia. [2]Department of Radiation Oncology, Netherlands Cancer Institute, Amsterdam 1066CX, The Netherlands.

E-mail: ricky.obrien@sydney.edu.au

Abstract. Four dimensional cone beam computed tomography (4DCBCT) uses a constant gantry speed and imaging frequency that are independent of the patient's breathing rate. Using a technique called Respiratory Motion Guided 4DCBCT (RMG-4DCBCT), we have previously demonstrated that by varying the gantry speed and imaging frequency, in response to changes in the patient's real-time respiratory signal, the imaging dose can be reduced by 50-70%. RMG-4DCBCT optimally computes a patient specific gantry trajectory to eliminate streaking artefacts and projection clustering that is inherent in 4DCBCT imaging. The gantry trajectory is continuously updated as projection data is acquired and the patient's breathing changes. The aim of this study was to realise RMG-4DCBCT for the first time on a linear accelerator.

To change the gantry speed in real-time a potentiometer under microcontroller control was used to adjust the current supplied to an Elekta Synergy's gantry motor. A real-time feedback loop was developed on the microcontroller to modulate the gantry speed and projection acquisition in response to the real-time respiratory signal so that either 40, RMG-4DCBCT$_{40}$, or 60, RMG-4DCBCT$_{60}$, uniformly spaced projections were acquired in 10 phase bins. Images of the CIRS dynamic Thorax phantom were acquired with sinusoidal breathing periods ranging from 2s to 8s together with two breathing traces from lung cancer patients. Image quality was assessed using the contrast to noise ratio (CNR) and edge response width (ERW).

For the average patient, with a 3.8s breathing period, the imaging time and image dose were reduced by 37% and 70% respectively. Across all respiratory rates, RMG-4DCBCT$_{40}$ had a CNR in the range of 6.5 to 7.5, and RMG-4DCBCT$_{60}$ had a CNR between 8.7 and 9.7, indicating that RMG-4DCBCT allows consistent and controllable CNR. In comparison, the CNR for conventional 4DCBCT drops from 20.4 to 6.2 as the breathing rate increases from 2s to 8s. With RMG-4DCBCT, the ERW in the direction of motion of the imaging insert decreases from 2.1mm to 1.1mm as the breathing rate increases from 2s to 8s while for conventional 4DCBCT the ERW increases from 1.9mm to 2.5mm.

Image quality can be controlled during 4DCBCT acquisition by varying the gantry speed and the projection acquisition in response to the patient's real-time respiratory signal. However, although the image sharpness, i.e., ERW, is improved with RMG-4DCBCT, the ERW depends on the patient's breathing rate and breathing regularity.

1. Introduction

Four dimensional cone beam computed tomography (4DCBCT) acquires volumetric images of a patient's anatomy in around ten different phases of the respiratory cycle (Taguchi 2003) and (Sonke et al. 2005). The utilisation of 4DCBCT imaging has grown steadily since the first commercial release by Elekta in 2009. To acquire the raw projection data, a constant gantry speed and constant projection frame rate are used. Unfortunately, for a majority of patients, the gantry speed used leads to slower acquisition times and higher imaging doses than are necessary, see Figure 1. In existing systems there is no active use of the respiratory signal to personalise the image acquisition, with the gantry speed selected so that adequate image quality is obtained for a wide range of patient breathing rates. The approach that we will explore in this papers is to personalise the image acquisition for each patient's unique breathing pattern.

We have previously published two approaches to reduce the imaging dose, imaging time and improve image quality (Cooper et al. 2013) and (O'Brien et al. 2013). The first technique, called respiratory triggered 4DCBCT (RT-4DCBCT), eliminates projection clusters (i.e., projections acquired with similar gantry angles), by suppressing redundant projections if a projection has already been acquired in the current respiratory bin (Cooper et al. 2013) and (Cooper et al. 2015). RT-4DCBCT reduces the imaging dose by an average of 50%, (Cooper et al. 2013), and was reduced to practice on an Elekta Synergy linear accelerator in 2015 (O'Brien et al. 2016).

As an example of RT-4DCBCT, in the first polar plot in Figure 1, only one projection in each cluster would be acquired; i.e., 45 projections would be acquired in total. Although, RT-4DCBCT reduces the imaging dose with only a small reduction in the image quality, for both conventional 4DCBCT and RT-4DCBCT the image quality, i.e., number of projection per phase, depends on the patient's breathing rate which leads to inconsistent image quality from patient to patient. Specifically, 120, 60, 40 and 30 projections are acquire for patients with 2, 4, 6 and 8 second breathing periods respectively with significantly different contrast to noise ratios resulting depending on the patient's breathing period. In addition, 4DCBCT is under sampled and is therefore susceptible to streaking artefacts which can be worse for patients breathing irregularly.

The second approach to improve image quality, called Respiratory motion guided 4DCBCT (RMG-4DCBCT), addresses the image quality shortcomings of RT-4DCBCT by also varying the gantry speed in real-time in response to the patient's real-time respiratory signal (O'Brien et al. 2013) and (O'Brien, Cooper, Kipritidis, Shieh & Keall 2014). As a simplified example, if the patient breathes faster than expected, we might increase the speed of the gantry and bring forward acquisition of the next projection. Similarly, if at a later stage the patient starts breathing slower, we might delay projection acquisition and slow the speed of the gantry.

In practice, RMG-4DCBCT utilises mathematical optimisation techniques to handle the complex task of acquiring evenly spaced projections simultaneously across ten or more respiratory phases without performing multiple gantry rotations (O'Brien,

Cooper, Kipritidis, Shieh & Keall 2014). RMG-4DCBCT allows the user to control image quality by obtaining images with a specified number of projections per respiratory phase which leads to a predictable contrast to noise ratio in the resulting images. Our aim in this study was to realise variable gantry speed image acquisition for the first time on a linear accelerator and to assess the resulting image quality and image sharpness.

2. Method

All experiments were performed on the research Elekta Synergy linear accelerator at the Netherlands Cancer Institute (NKI). Our real-time software controls the gantry rotation speed and suppresses triggers to the kV source so that a specified number of evenly spaced projections were acquired in each respiratory phase. For example, if a clinical application requires 40 projections in each of 10 respiratory phases, then the gantry speed was adjusted in real-time so that the 40 full fan projections per phase were evenly spaced around a 200 degree arc in each of the ten phase bins (400 projections in total). One projection per respiratory phase was acquired in each respiratory cycle so the imaging time was 40 respiratory cycles.

2.1. Suppressing redundant projections

Suppressing projections was accomplished with the use of an electromagnetic relay to suppress projection triggers to the kV source while the detector was read at a fixed frame rate of 5.5Hz. If the relay was closed then projection pulses could reach the kV source and the detector read out a projection. If the relay was open the kV triggering of the source is prevented and the detector reads out a dark frame that is discarded from image reconstruction. The relay switching was perform with a control system programmed on a microcontroller (168Mhz 32-bit Cortex-M4) that received real-time input from a respiratory sensor during image acquisition. The relay electronically isolates the control system from the linear accelerator's circuitry, making the whole system safer. The real-time control system acquired projections as close to the centre of each respiratory phase as possible, which measurably increases the image sharpness and reduces motion blur (O'Brien et al. 2016). Full details on the circuitry, implementation and handling of latencies can be found in (O'Brien et al. 2016) and the method used to correct for image lag can be found in (Stankovic et al. 2016).

2.2. Realising variable gantry speed 4DCBCT

The Elekta imaging software, XVI, was set-up in IntraFractionImaging mode with the MV beam off to accelerate the gantry to $3.3°/s$ over $10°$ and then to acquire kV images at 5.5Hz over a $200°$ arc in 60 seconds with a further $10°$ arc at the end to decelerate the gantry to a stationary position. As soon as the gantry reaches $3.3°/s$, our software starts adjusting the gantry speed in response to the patient's real-time respiratory signal as described below.

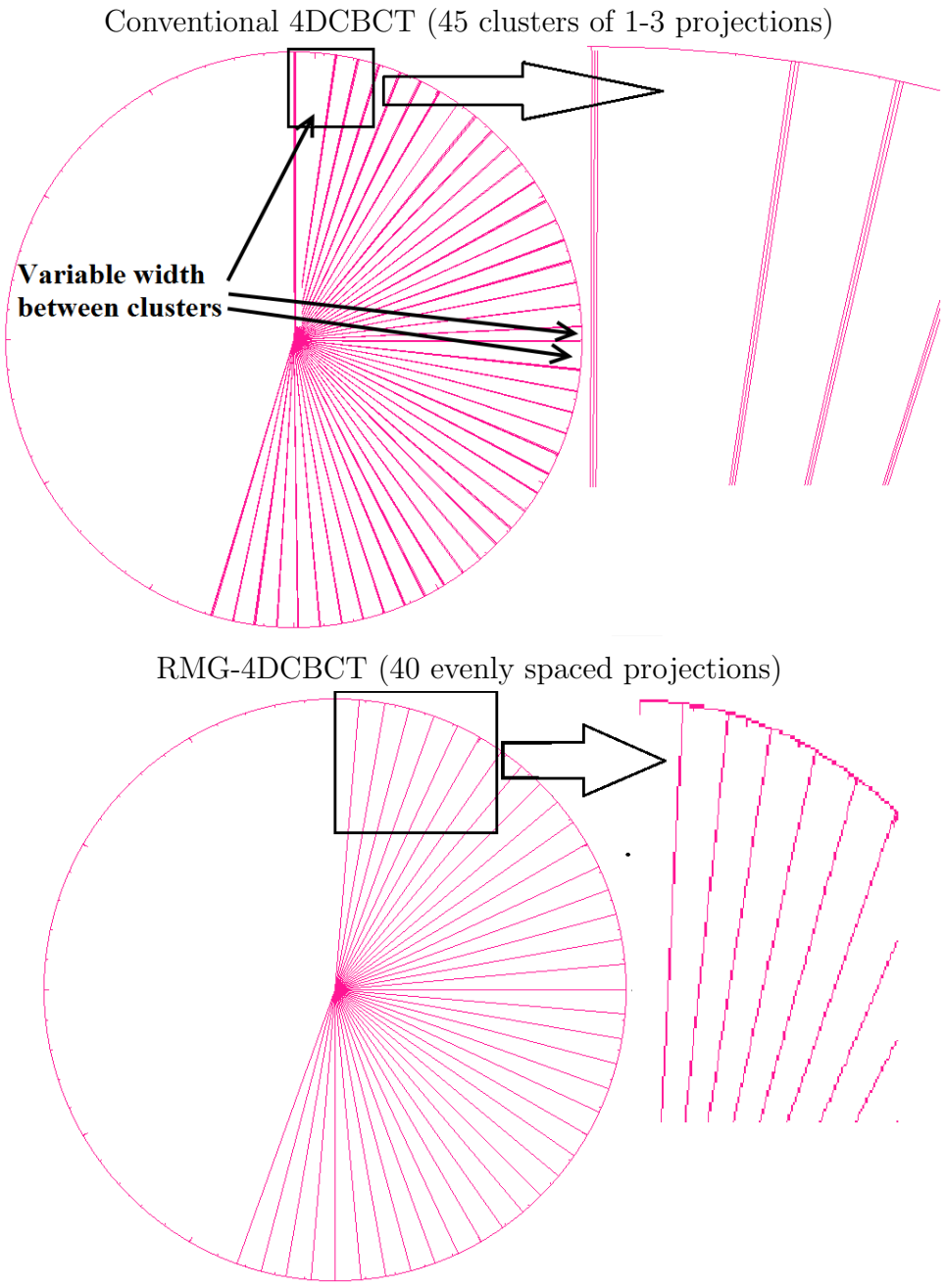

Figure 1. Polar plots of the gantry angle for each projection acquired with conventional 4DCBCT and RMG-4DCBCT for a lung cancer patient. For this patient's breathing rate, conventional 4DCBCT acquires 138 projections in 45 clusters. RMG-4DCBCT acquires 40 uniformly spaced projections (71% dose reduction) by modulating the gantry speed and kV acquisition in response to the patient's real-time respiratory signal.

2.2.1. Adjusting the gantry speed: A potentiometer, or variable resistor, was connected in series with a wire used to control the gantry speed, see Figure 2. The resistance of the potentiometer was adjusted by turning the potentiometers wiper with a DC

Gantry control circuit

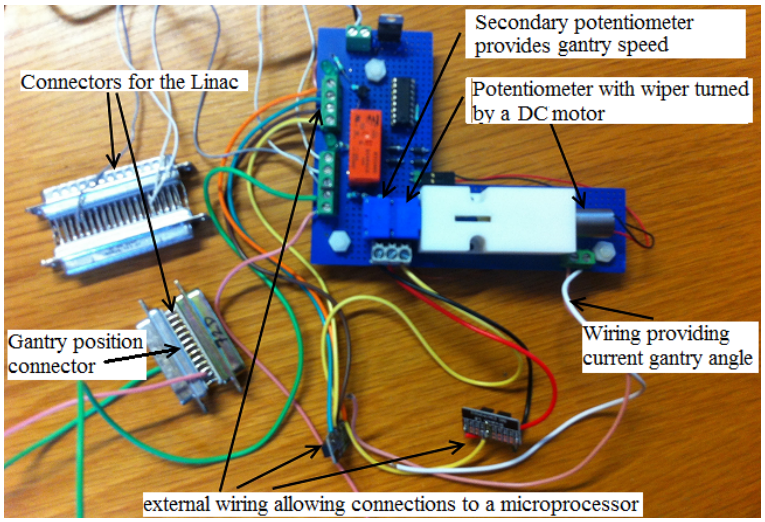

Connections to Linac

Suppressing kV projections

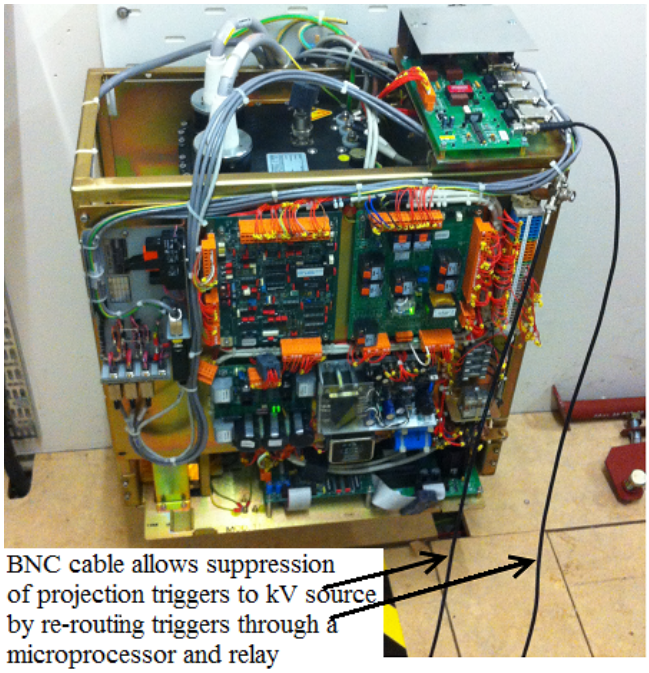

Figure 2. Top: The circuitry used to control the gantry speed. Bottom Left: The device controlling the gantry speed connected to the Linac. Bottom Right: The connections required to suppress projection triggers to the kV source, see (O'Brien et al. 2016).

motor which changes the current on the wire and hence the gantry speed. By turning the potentiometers wiper physically rather than electronically, i.e., by turning the potentiometer with a DC motor rather than a digital potentiometer, we were able to electronically isolate our microcontroller from the linear accelerator's control system which leads to a safer design.

For safety reasons, the International Electrotechnical Commission (I.E.C) specifies a maximum gantry velocity of $6^\circ/s$ for linear accelerators. Analysis of the log files produced by our microcontroller indicates that the linear accelerator was only requested to exceed $3^\circ/s$ for 0.5% of the time for the lung cancer patient breathing traces. At no point during image acquisition was the linear accelerator requested to exceed $5^\circ/s$.

The Elekta Synergy linear accelerator has an acceleration and deceleration that depends on the gantry angle with an acceleration ranging from $1.8^\circ/s^2$ to $3.2^\circ/s^2$ and a deceleration ranging from $3.4^\circ/s^2$ to $4.3^\circ/s^2$ (Boylan et al. 2011). Requesting an acceleration above the physical capabilities of the system will result in the system not being able to keep up which will lead to small gantry position errors. Analysis of our log files reveals that the requested acceleration/deceleration was below $2^\circ/s^2$ for 94% of the time with an acceleration/deceleration above $4^\circ/s^2$ requested 3.7% of the time.

2.2.2. Calibration procedure for gantry speed control: A feedback loop was realised by connecting a secondary potentiometer to the first potentiometer so that the speed of the gantry can be monitored in real-time, see Figure 2. An analogue pin on the microcontroller was used to measure the output voltage from the secondary potentiometer. To calibrate the secondary potentiometers output to the gantry speed, we rotated the gantry with various wiper locations (i.e., various positions of the first potentiometer) then measured the voltage on the secondary potentiometer and the time required to rotate the gantry 180°. This data was used to compute the gantry speed as a function of the output voltage on the secondary potentiometer. An exponential curve was used to fit the data to give an equation for the voltage, V, as a function of the gantry speed, S:

$$V = -1.006 \ln (0.1795S). \tag{1}$$

The voltage required for a desired gantry speed was calculated using equation 1 and the potentiometers wiper was turned until the output voltage on the secondary potentiometer was within 0.05 volts of the desired voltage.

2.2.3. Determining the real-time gantry position: The Elekta control system uses the gantry position at various locations within their system and we were able to find a convenient location to extract the gantry position signal, see the connectors labelled in Figure 2. For this connection, the voltage on the wire changed linearly with gantry position so we were able to keep track of the gantry position at all times with a simple linear relationship between voltage and position.

Although the voltage on the signal wire rises linearly with gantry angle, there were small deviations from a linear relationship which led to errors in the gantry angle used by our microcontroller. The error in the gantry angle between the value that we read from the signal wire and the value displayed on the console by the linear accelerator was at most 0.5 degrees over the arc used to acquire our 4DCBCT scans.

2.2.4. Calculating the new gantry speed: The real-time gantry position, the real-time respiratory signal and the number of projections acquired to date were used to compute the new gantry speed every time a projection was acquired. With limited computational power available on the microcontroller (168MHz), we chose to use a simple algorithm to compute the instantaneous gantry speed rather than the more computational intensive algorithms that we have previously published (O'Brien et al. 2013) and (O'Brien, Cooper, Kipritidis, Shieh & Keall 2014). The simple algorithm determines where the gantry should be one breathing cycle ahead and then computes the velocity required to reach that location by the next breathing cycle. A flowchart of the algorithm is given in Figure 3.

2.3. CIRS imaging phantom, breathing traces and image reconstruction

The CIRS dynamic thorax phantom model 008A (Computerized Image Reference System Inc, USA) was used for all experiments with the 3cm spherical imaging insert placed in the phantom. Two cm peak-to-peak sinusoidal breathing traces (i.e., 1cm amplitude) in the superior-inferior direction were used with breathing periods ranging from 2, 4 and 8 seconds. To represent the case where the patient spends longer in exhale, we have used a breathing trace of the form $\cos^6$ as described in (Lujan et al. 1999).

To model an extreme situation where the patient's breathing rate continuously changes, a sinusoidal breathing trace was used where the breathing period decreased linearly from 8 seconds to 2 seconds over a period of 4 minutes. Finally, two respiratory traces from lung cancer patients, from the study of (George et al. 2006), which were acquired using the Real-time Position Management (RPM) system from Varian Medical Systems, were also programmed into the CIRS phantom to represent real patient breathing data. The motion of the phantom's imaging insert is in the SI direction and theses breathing traces are plotted in Figure 4.

2.4. Real-time phase calculation

In conventional 4DCBCT and 4DCT applications the phase signal is computed retrospectively from the respiratory signal extracted from an external sensor, such as the RPM system from Varian Medical Systems, or from the images themselves (Zijp et al. 2004) and (Yan et al. 2013). In order to acquire projections in phase bins, RMG-4DCBCT needs to know the phase of the breathing signal in real-time as new respiratory data arrives. For the sinusoidal and cosine breathing traces, the real-time phase was calculated by monitoring five respiratory cycles to determine the average breathing period and then the peaks in the signal were used to linearly extrapolate the phase, see (O'Brien et al. 2016) for more details.

For the linearly decreasing period and the patient breathing traces, the real-time phase was calculated using the real-time method of Ruan (Ruan et al. 2009). To make a fair comparison with current practice for conventional 4DCBCT, the phase in the conventional 4DCBCT simulations was computed by retrospectively detecting the

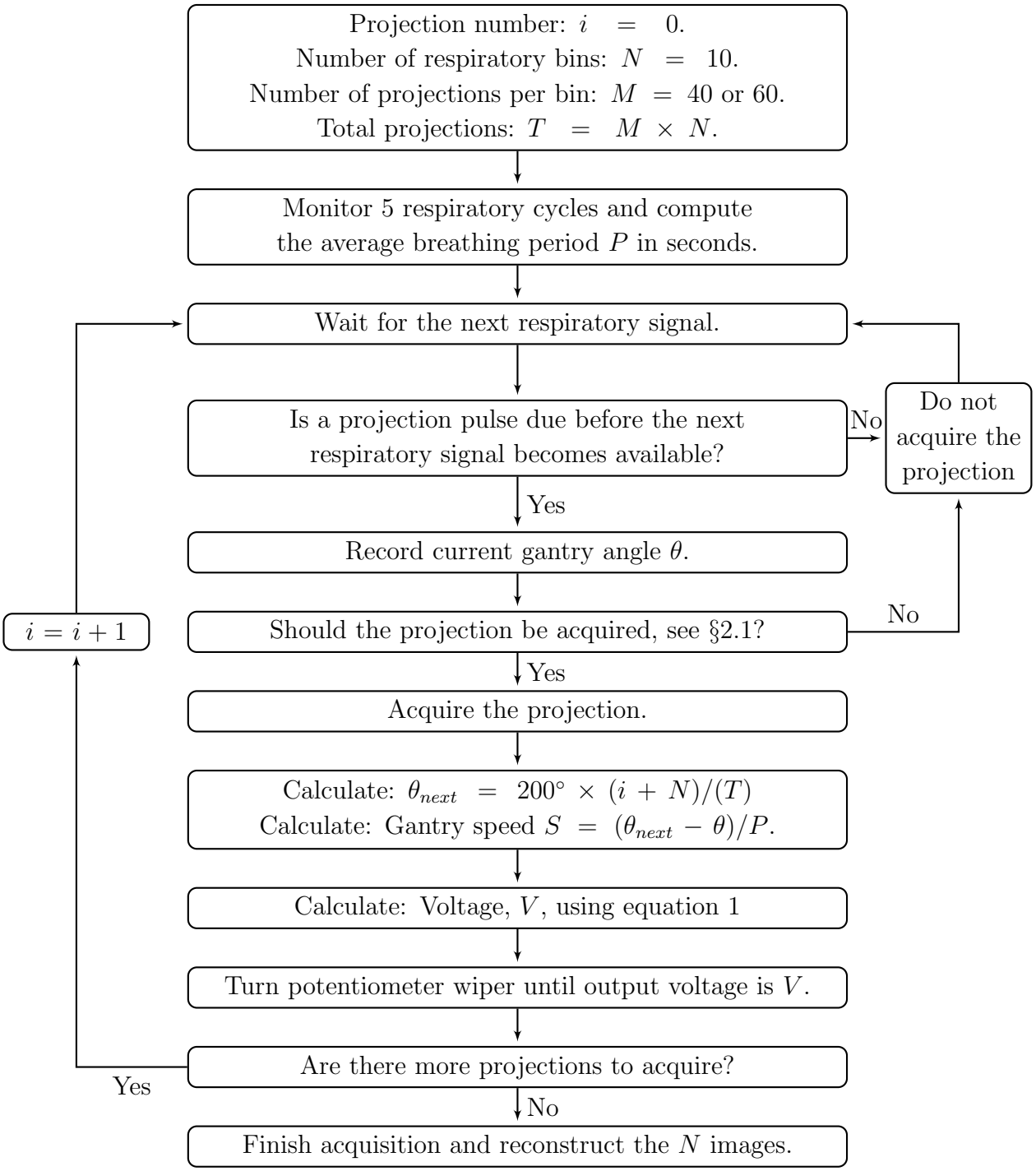

Figure 3. A flowchart showing the main algorithm used on the microcontroller to adjust the gantry speed in real-time and to acquire the projections.

inhale peaks in the respiratory signal with the phase rising linearly from peak inhale to peak inhale. Using this approach, our results compare projections acquired with RMG-4DCBCT using a real-time phase signal to those obtained using current best practice where the phase is computed retrospectively.

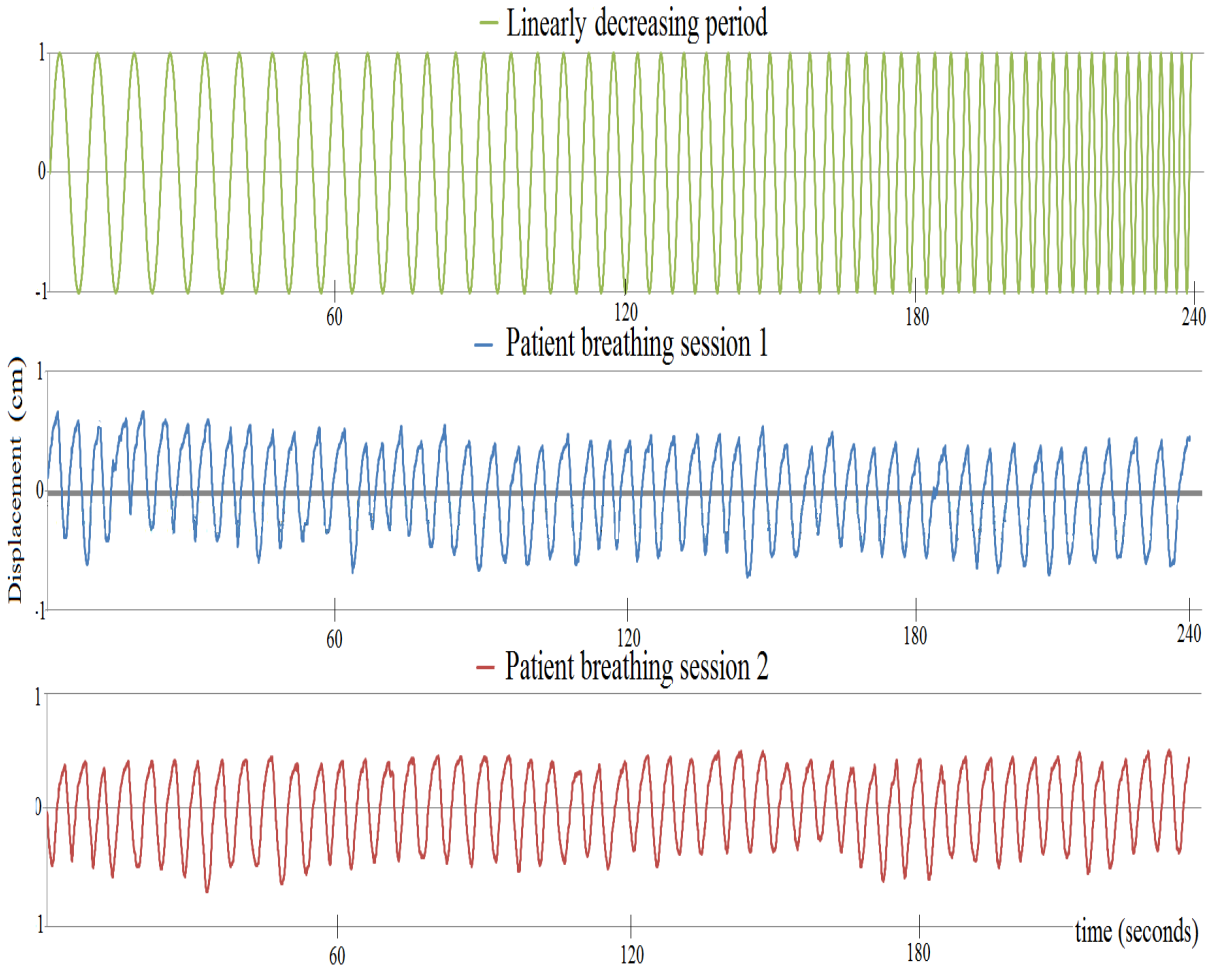

Figure 4. The breathing traces used in addition to sinusoidal motion; the motion is in the SI direction for our experiments. Top: A sinusoidal breathing trace with the period reducing from 8 seconds to 2 seconds over 4 minutes. Middle: The first breathing trace from a lung cancer patient (Breathing period is 4.7 ± 0.5s). Bottom: The second breathing trace from a lung cancer patient (Breathing period is 4.8 ± 0.4s).

2.5. Image quality metrics: Contrast to Noise Ratio (CNR) and Edge Response Width (ERW)

We have used the contrast to noise ratio (CNR) to quantify image contrast. The CNR was computed using:

$$CNR = |\bar{I}_{tissue} - \bar{I}_{lung}|/\sigma_{tissue},$$

where $\bar{I}_{tissue}$ and $\bar{I}_{lung}$ are the mean of the voxels intensities over a 1cm^3 region of static tissue and static lung respectively and σ_{tissue} is the standard deviation of the tissue intensity in the same 1cm^3 region of tissue.

The edge response width (ERW) was used to measure image sharpness. The spatial

distance, in mm, for the signal to rise from 25% to 75% of the difference between the intensity of the lung and tissue was computed from the reconstructed images in the LR and SI directions at the widest point of the spherical insert. The ERW was calculated on both sides of the imaging insert for all ten phase bins to give 20 separate ERW values which were averaged for each reconstruction. More details on computing the ERW can be found in (Shieh et al. 2014).

Although streaking can affect the ERW, a smaller ERW usually suggests that the edges of features in the reconstructed image are more clearly defined. As there was no motion of the sperical insert in the AP and LR directions, the ERW in the LR direction represents the ERW obtained on stationary anatomy with the ERW. There was motion of the sperical insert in the SI direction, so the increase in the ERW in the SI direction over the LR direction is a metric that we will use to measure the contribution of motion to the blurring of anatomical features within each phase bin.

2.6. 4DCBCT acquisition methods

Three 4DCBCT acquisition methods were used:

- RMG-4DCBCT$_{40}$ and RMG-4DCBCT$_{60}$ which used both projection suppression and gantry control to acquire 40 and 60 projections respectively per respiratory phase bin. The choice of 40 projections per phase corresponds to the number of projection clusters that are acquired with conventional 4DCBCT for a patient with a 6 second breathing period and 60 corresponds to a 4 second breathing period. The aim was to acquire 400 or 600 projections in total across 10 respiratory phases.
- Conventional 4DCBCT which acquired 1320 projections over 4 minutes. The phase was retrospectively determined from the respiratory signal and projections were post processed into 10 respiratory phase bins.

For all acquisitions a maximum frame rate of 5.5Hz was used to acquire full fan projections over 180° plus the fan angle, i.e., 200°, at 120 kVp, 0.8×0.8mm pixel size and a 20ms exposure time. The scans were acquired in IntraFractionImaging mode so that the speed of the gantry could be changed during image acquisition.

2.7. Image reconstruction

Images were reconstructed using the FDK algorithm (Feldkamp et al. 1984) from the Reconstruction Tool Kit (Rit et al. 2014) using $256 \times 256 \times 256$ voxels of size 1mm^3.

3. Results

3.1. Imaging dose and acquisition time

Table 1 lists the number of projection acquired, the reduction in the imaging dose compared to conventional 4DCBCT, i.e., the total number of projections acquired, and the reduction in the image acquisition time for RMG-4DCBCT$_{40}$ and RMG-4DCBCT$_{60}$.

Table 1. The total number of projections and the total image acquisition time for the different 4DCBCT methods. The percentages in brackets represent the reduction, or increase for negative numbers, over the corresponding conventional 4DCBCT acquisition. Note: The imaging dose here is a first order approximation to the imaging dose as we are measuring imaging dose by the number of projections acquired.

	RMG-4DCBCT$_{40}$		RMG-4DCBCT$_{60}$		Conventional	
Breathing	#	Time	#	Time	#	Time
Trace	Proj's	(sec)	Proj's	(sec)	Proj's	(sec)
Sin 2 sec	426(68%)	88(63%)	633(52%)	131(45%)	1320	240
Sin 4 sec	398(70%)	158(34%)	592(55%)	239(0%)	1320	240
Sin 8 sec	399(70%)	316(-31%)	565(57%)	449(-87%)	1320	240
Cos^6 4 sec	398(70%)	159(34%)	596(55%)	238(0%)	1320	240
Linear decreasing	401(70%)	164(32%)	593(55%)	274(-14%)	1320	240
Patient 1	399(70%)	203(15%)	581(56%)	312(-30%)	1320	240
Patient 2	400(70%)	203(15%)	586(56%)	305(-27%)	1320	240

RMG-4DCBCT$_{40}$ reduces the imaging dose by 70% while RMG-4DCBCT$_{60}$ reduces the image dose by 55% when compared to conventional 4DCBCT. As the image acquisition time is the breathing period multiplied by the number of projections per respiratory phase, the imaging time for RMG-4DCBCT increases for slower breathing patients; the imaging time exceeds the 4 minute conventional 4DCBCT scan for a patient with a 6 second breathing period with RMG-4DCBCT$_{40}$ and a patient with a 4 second breathing period with RMG-4DCBCT$_{60}$. It should be noted that in these cases the image quality will be better with RMG-4DCBCT because conventional 4DCBCT will not acquire a large number of projection clusters.

Note that in our current proof of principle study, RMG-4DCBCT$_{40}$ did not always acquire exactly 400 projections. This was a result of small errors in the gantry angle and gantry velocity control loop. In more detail, the gantry was started at -40° and stopped at 180° with the XVI system automatically acquiring projections when the gantry was between $-30°$ and 170°. The 10 degree buffer was to allow the gantry to accelerate/decelerate to speed before/after image acquisition. As the gantry approaches -30°, noise in the gantry angle signal on our microcontroller did not always match up perfectly with the Elekta control systems gantry angle signal so the image acquisition sometimes started a little before or a little after our microcontroller anticipated. A similar situation occurred as the gantry approached the end of acquisition, at 170°, with the system ceasing acquisition a little before or a little after our microcontroller anticipated. For the 2 second breathing period, where the gantry was moving faster, this resulted in more projections than anticipated, while for the slower breathing rates fewer projections than anticipated were acquired, see the projection totals in Figure 5.

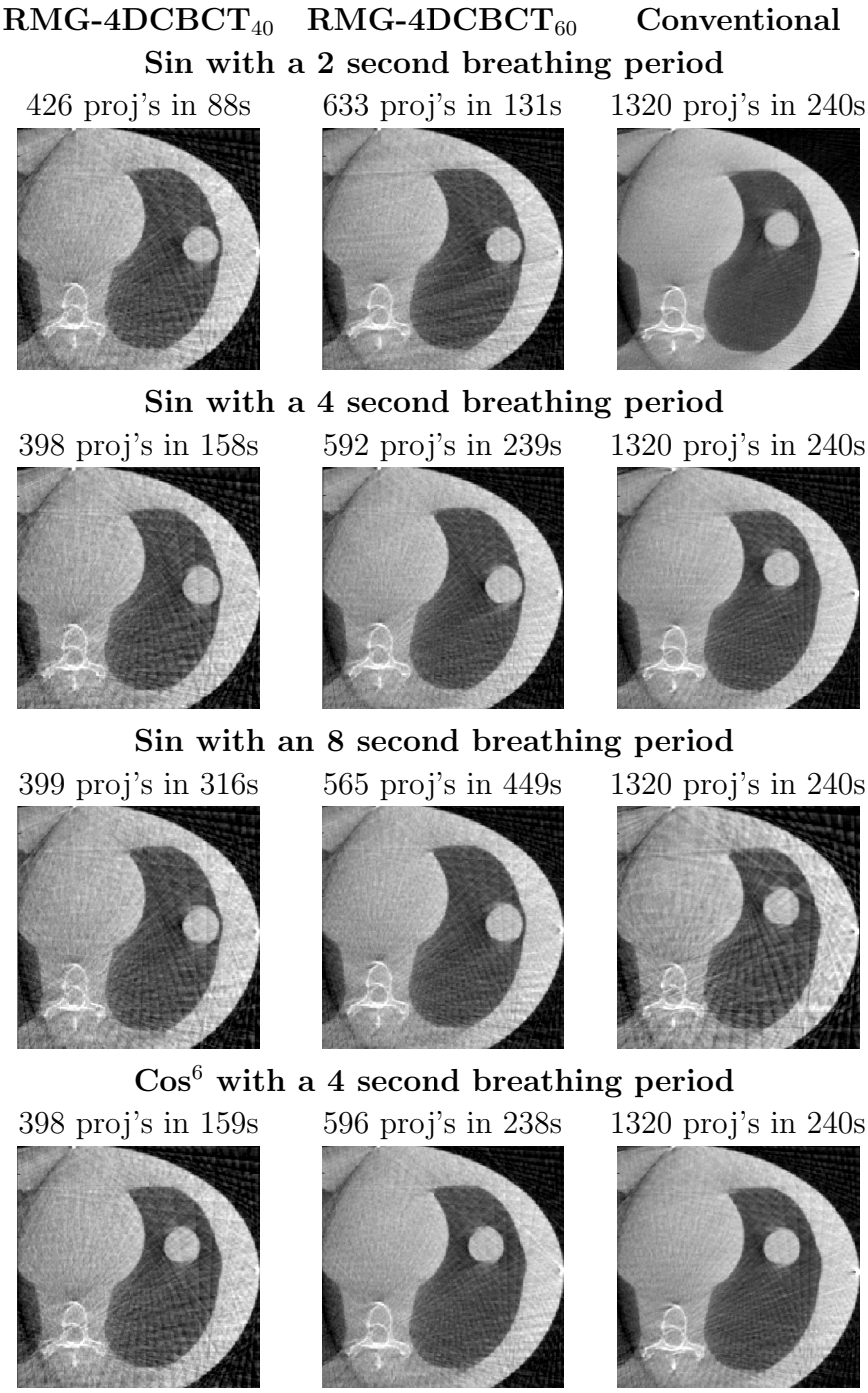

Figure 5. A transverse slice of the peak inhale phase bin with RMG-4DCBCT$_{40}$, RMG-4DCBCT$_{60}$ and conventional 4DCBCT for a variety of different sinusoidal breathing rates. Also listed are the total number of projections across all 10 phase bins and the image acquisition time.

3.2. Reconstructed images

Figure 5 displays a transverse slice for the different image acquisition protocols. Visually, the image quality for RMG-4DCBCT$_{40}$ and RMG-4DCBCT$_{60}$ are consistent regardless

of the breathing rate while the image quality for conventional 4DCBCT varies with the breathing.

Figure 6 displays a transverse slice for the linearly decreasing period and the two patient breathing traces. As conventional 4DCBCT uses a retrospectively computed phase and RMG-4DCBCT used a real-time phase algorithm, these images represent a realistic comparison between current practice and RMG-4DCBCT. As was the case for the sinusoidal breathing traces, image quality is consistent regardless of the breathing period with RMG-4DCBCT, while for conventional 4DCBCT the image quality varies depending on the breathing period with faster breathing patients having better image quality. For the linearly decreasing period, conventional 4DCBCT has light streaking that is variable in width which reflects the decrease in the patient breathing period during the four minute scan; these streaks were reduced using RMG-4DCBCT.

3.3. Image contrast (The CNR ratio)

The CNR for all image reconstructions are given in Figure 7. For RMG-4DCBCT, the CNR is between 6.5 and 7.5 with RMG-4DCBCT$_{40}$ and between 8.7 and 9.7 with RMG-4DCBCT$_{60}$. For conventional 4DCBCT, the CNR depends on the total number of projection clusters with a higher CNR when there are more projection clusters for faster breathing patients. For the 2s breathing period, there are approximately 120 projection clusters and the CNR is 20.4. The CNR drops to 6.2 for the 8s breathing period where only 30 projection clusters are obtained.

3.4. Image sharpness (The Edge Response Width ERW)

Figure 8 gives the ERW in the LR direction for all images reconstructed. There was no motion of the imaging insert in the LR and AP directions, so the ERW is smaller when there are fewer streaks in the image near the imaging insert. For example, for conventional 4DCBCT, the ERW is larger for the 8s breathing period, with a very high standard deviation, than the 2s breathing period because there are more streaks for the 8s breathing period. There is very little difference in the ERW when comparing RMG-4DCBCT$_{40}$ to RMG-4DCBCT$_{60}$ and the small variations usually reflecting the location of streaks near the imaging insert. This suggests that as far as the ERW is concerned, in regions with little motion, there is not a noticeable benefit in using RMG-4DCBCT$_{40}$ over RMG-4DCBCT$_{60}$. However, conventional 4DCBCT has a higher ERW, and a very large variation in the ERW, for the 8 second breathing period because of the severe under sampling making the reconstructed images more susceptible to streaking artefacts.

Analysing the ERW in the SI direction is more complicated than in the LR direction because motion of the imaging insert increases the ERW by up to 1.5mm; i.e., compare Figure 8 to Figure 9. In general, the ERW will be smaller if the projections are acquired closer to the centre of the respiratory phase bin; i.e., there is a smaller intra phase bin displacement variation of the imaging insert.

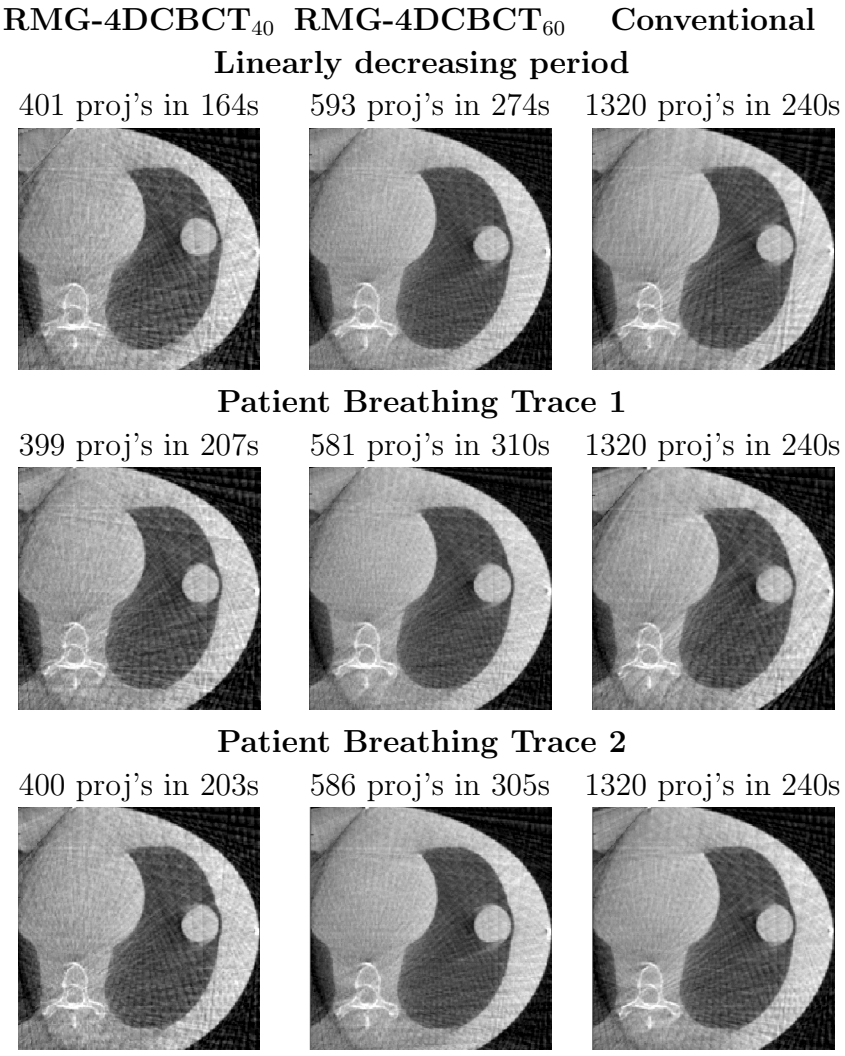

Figure 6. A transverse slice of the peak inhale phase bin with RMG-4DCBCT$_{40}$, RMG-4DCBCT$_{60}$ and conventional 4DCBCT for the two patient breathing traces and the linearly decreasing breathing period. Conventional 4DCBCT used the phase that was retrospectively extracted from the motion of the insert while the two RMG-4DCBCT simulations used the Ruan real-time phase algorithm. Also listed are the total number of projections across all 10 phase bins and the image acquisition time.

For the sinusoidal breathing traces with RMG-4DCBCT, the ERW is smaller for slower breathing patients because it is easier to select the projection closer to the centre of the respiratory phase bin when suppressing projections. As the ERW is primarily dominated by the breathing period, we do not expect a big difference between RMG-4DCBCT$_{40}$ and RMG-4DCBCT$_{60}$ which is confirmed in our results with RMG-4DCBCT$_{40}$ sometimes performing better and sometimes worse than RMG-4DCBCT$_{60}$. For conventional 4DCBCT the ERW increases with the patient's breathing period as there are a larger number of projections in each projection cluster.

The linear decreasing period and the two patient breathing traces compare the

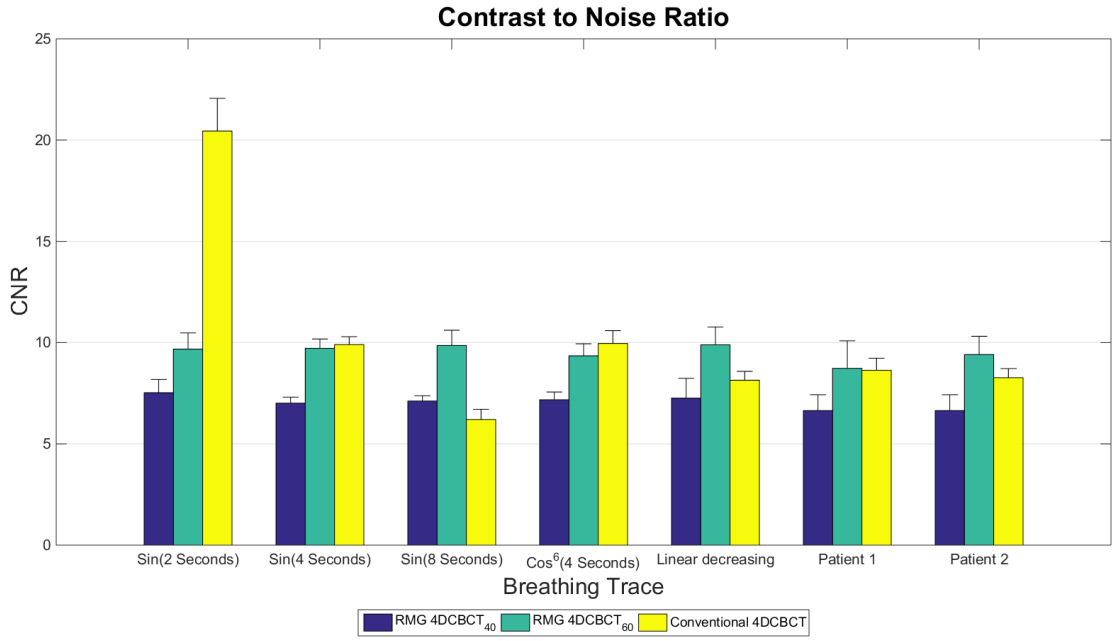

Figure 7. The mean, coloured bars, and standard deviation, error bars, across the 10 phase bins of the CNR. The CNR depends on the total number of projection clusters per respiratory phase bin.

retrospectively computed phase for conventional 4DCBCT to the real-time phase algorithms for RMG-4DCBCT. Our results indicate that the ERW for real patient data is larger than for the sinusoidal breathing traces which is expected due to irregularities in real patient breathing rates.

The Ruan real-time phase method produces an ERW that is smaller than the retrospectively binned conventional 4DCBCT. For patient 1, there is more irregularity in the amplitude peaks than for patient 2, see Figure 4, which may explain why patient 1 has a larger ERW than patient 2.

4. Discussion

We have implemented RMG-4DCBCT for the first time on a linear accelerator and demonstrated that the gantry speed and kV acquisition can be controlled in real-time in response to the patient's real-time respiratory signal. In this proof of principle study, our implementation of the gantry control algorithm was a simplified version of the more complicated gantry control algorithms as described in our previous publication (O'Brien, Cooper, Kipritidis, Shieh & Keall 2014) yet despite these simplifications clinically useful images were obtained on lung cancer patient breathing traces.

We anticipate a further second order improvement if we implement the more complicated gantry control algorithms and reduce the noise in the sensors used in our real-time control circuit. The more complicated gantry control algorithms allow us to

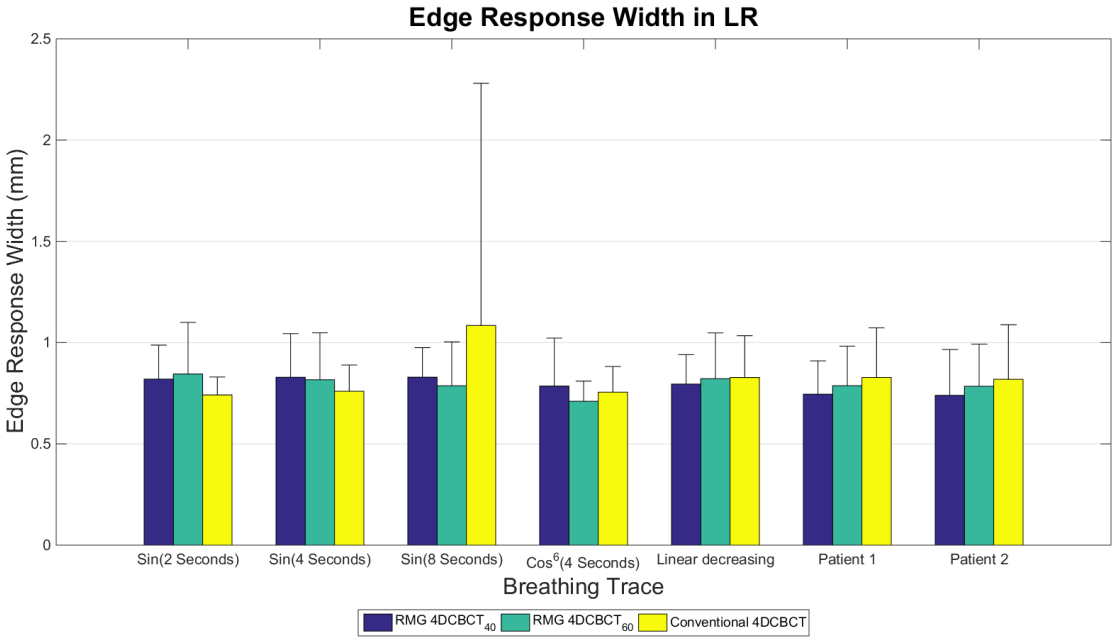

Figure 8. The mean, coloured bars, and standard deviation, error bars, across the 10 phase bins of the edge response width (ERW) in LR. There is no motion in the LR direction so the ERW is influenced by the amount of streaking near the 3cm imaging insert.

better handle the gantry acceleration and velocity limits and ensure that the acceleration limits are not exceeded which is of particular importance for irregular and fast breathing patients and would help to reduce wear and tear on the linear accelerators gantry motor.

In addition to implementing RMG-4DCBCT for the first time, this was the first study to compare retrospectively binned conventional 4DCBCT to 4DCBCT images binned with a real-time phase algorithm. For the patient breathing traces in Figure 9, our results demonstrated that the real-time phase algorithm produced a smaller ERW than the retrospectively binned experiments. This improvement is either a result of a reduction in the intra phase bin displacement variation of the acquired projections or a result of the different interpretation of what phase is between the Ruan approach and the conventional approach. In the Ruan phase calculation, a 'natural' or mathematical phase for the system is extracted and a consequence of this is that for patients holding their breath the phase stops increasing. For most phase calculation algorithms that are published in the literature, the phase increases linearly in time, so if the patient holds their breath then the phase continues to increase; a study into the influence of phase calculation methods on the reconstructed images is warranted and any progress towards eliminating the need to compute phase, e.g. with displacement binning, would be beneficial.

Our results indicate that image quality can be controlled with RMG-4DCBCT by defining the number of projections per phase bin that are required for the given clinical

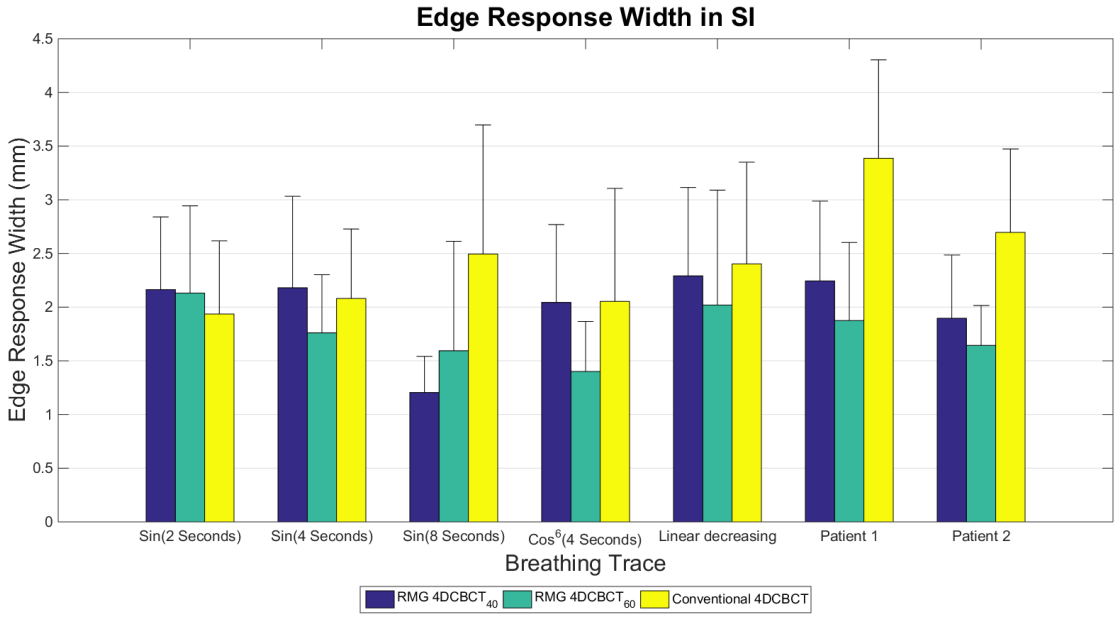

Figure 9. The mean, coloured bars, and standard deviation, error bars, across the 10 phase bins of the edge response width (ERW) in SI. Due to the motion of the imaging insert in the SI direction, the ERW depends on the patient's breathing rate, and the method used to calculate the respiratory phase.

application. However, despite the ERW being smaller on average using RMG-4DCBCT than when using conventional 4DCBCT, the image sharpness cannot be controlled completely in the SI direction. As the ERW is a factor in regards to the accuracy of segmentation, delineation and registration of images, it is desirable to develop this work further so that the segmentation, delineation and registration errors can be controlled. We observed that the ERW in SI was influenced by the patient's breathing period, irregularity in the breathing amplitude and any baseline drifts in the breathing signal.

The main drawback of RMG-4DCBCT is that the imaging time depends on the patient's breathing rate. RMG-4DCBCT will acquire the projections in the minimum amount of time possible for the given patient's breathing rate. However, if the scan time is predicted to be too long for a slow breathing patient, then the operator will need to weigh up the benefit of reducing the image quality, i.e., number of projections per phase, with the expected clinical benefit to the patient.

Our experiments in this study only included two breathing traces from lung cancer patients. A previous RMG-4DCBCT study covers irregular breathing patients in more detail using a simulated RMG-4DCBCT and linac system (O'Brien, Cooper, Kipritidis, Shieh & Keall 2014) which used 112 breathing traces from 24 lung cancer patients. The average breathing period of the 24 lung cancer patients was 3.8s, (George et al. 2005), which corresponds to an image acquisition time of 152 seconds for 40 projections per respiratory phase (a 37% reduction in acquisition time). The 5^{th} and 95^{th} percentile

range in breathing period were 2.1 to 6.7 seconds which corresponds to image acquisition times of between 84 and 268 seconds for 90% of lung cancer patients. It should be noted that these studies were limited to 24 lung cancer patients and it is not uncommon for patients to have slower or more irregular breathing rates than cited above. For these very slow, or irregular, breathing patients, RMG-4DCBCT will have slow acquisition times and conventional 4DCBCT will exhibit poor image quality. One possible solution is to use a system with a faster gantry rotation speed or even robotic C-Arm systems that are used in interventional surgery. Although there will be regulatory issues to overcome with faster rotation speeds, we have previously estimated that the imaging time can be reduced to 60 seconds for half fan acquisition and 30-40 seconds for full fan acquisition (O'Brien, Cooper, Kipritidis, Shieh & Keall 2014).

The closest approach to RMG-4DCBCT that has been published in the literature involves calculating the gantry rotation speed based on the average breathing period of the patient (Lu et al. 2007). RMG-4DCBCT has several differences to this approach: (1) RMG-4DCBCT eliminates clustering of projections and attempts to acquire the projection as close to the centre of the respiratory phase as possible. (2) There is a manual step required by the operator to calculate and set the gantry rotation speed before the scan starts. (3) When a constant gantry rotation speed is used, a buffer needs to be added to compensate for irregularities in the patient's breathing. For example, if the patient is likely to change their breathing rate by 25% from one breathing cycle to the next, then the gantry rotation speed will need to be 25% lower than we would calculate from the average breathing period; this increases imaging time and imaging dose. (4) RMG-4DCBCT is more robust to patient breathing irregularities.

There are other approaches that have been published in the literature to improve image quality with the most common approaches using iterative reconstruction techniques after the raw data has been acquired, see (Bian et al. 2010), (Bergner et al. 2009), (Bergner et al. 2010), (Leng et al. 2008), (Li et al. 2007), (Brehm et al. 2012), (Brehm et al. 2013), (O'Brien, Kipritidis, Shieh & Keall 2014) and (Mckinnon & Bates 1981) or techniques that attempt to reconstruct 4DCBCT from a one minute 3DCBCT (Yan et al. 2014). RMG-4DCBCT can be used in conjunction with these approaches but it has the added benefit that it is the only technique that addresses image quality and imaging dose issues at the source of the problem; i.e., during image acquisition. When RMG-4DCBCT is combined with these approaches we anticipate further imaging dose reductions and improved image quality.

5. Conclusions

We have reduced to practice a technique for varying the gantry speed during 4DCBCT image acquisition with the imaging dose reduced by 55-70% for all patients. Image quality can now be controlled during 4DCBCT acquisition except for the ERW which depends on the patient's breathing rate. For a given image quality, the images are acquired with the minimum imaging dose and the shortest acquisition time possible for

the patient's breathing rate. The total image acquisition time depends on the patient's breathing period with the raw projection data acquired faster for patient's with shorter breathing periods.

Acknowledgements and Disclosures

Professor Keall would like to acknowledge the support of a National Health and Medical Research Council (NHMRC) Australia Fellowship. This project was supported by a Cancer Australia Priority Driven Collaborative Cancer Research Scheme project grant number 1084566 and in part by NHMRC project grant 1034060. Dr Sonke would like to acknowledge research support from Elekta and that his department receives licensing fees from Elekta. We would like to thank the Engineers at NKI, in particular Reinoud Verkerk and Marco van den Berg, for their help in setting up the hardware and electronics for this project. This work is the topic of a patent filed by Professor Keall and Dr O'Brien for Variable gantry speed 4DCBCT image acquisition.

References

Bergner F, Berkus T, Oelhafen M, Kunz P, Pan T, Grimmer R, Ritschl L & Kachelriess M 2010 *Med Phys* **37**(9), 5044–53.

Bergner F, Berkus T, Oelhafen M, Kunz P, Pan T & Kachelriess M 2009 *Med Phys* **36**(12), 5695–706.

Bian J, Siewerdsen J H, Han X, Sidky E Y, Prince J L, Pelizzari C A & Pan X 2010 *Phys Med Biol* **55**(22), 6575–99.

Boylan C J, Rowbottom C G & Mackay R I 2011 *Physics in Medicine and Biology* **56**(13), 4119–4133.

Brehm M, Paysan P, Oelhafen M & Kachelriess M 2013 *Medical Physics* **40**(10).

Brehm M, Paysan P, Oelhafen M, Kunz P & Kachelriess M 2012 *Medical Physics* **39**(12), 7603–7618.

Cooper B J, O'Brien R T, Balik S, Hugo G D & Keall P J 2013 *Med Phys* **40**(4), 041901.

Cooper B J, O'Brien R T, Kipritidis J, Shieh C C & Keall P J 2015 *Phys Med Biol* .

Feldkamp L A, Davis L C & Kress J W 1984 *Journal of the Optical Society of America a-Optics Image Science and Vision* **1**(6), 612–619.

George R, Chung T D, Vedam S S, Ramakrishnan V, Mohan R, Weiss E & Keall P J 2006 *Int J Radiat Oncol Biol Phys* **65**(3), 924–33.

George R, Vedam S S, Chung T D, Ramakrishnan V & Keall P J 2005 *Medical Physics* **32**(9), 2850–2861.

Leng S, Tang J, Zambelli J, Nett B, Tolakanahalli R & Chen G H 2008 *Physics in Medicine and Biology* **53**(20), 5653–5673.

Li T, Koong A & Xing L 2007 *Med Phys* **34**(9), 3688–95.

Lu J, Guerrero T M, Munro P, Jeung A, Chi P C, Balter P, Zhu X R, Mohan R & Pan T 2007 *Med Phys* **34**(9), 3520–9.

Lujan A E, Larsen E W, Balter J M & Ten Haken R K 1999 *Med Phys* **26**(5), 715–20.

Mckinnon G C & Bates R H T 1981 *Ieee Transactions on Biomedical Engineering* **28**(2), 123–127.

O'Brien R T, Cooper B J & Keall P J 2013 *Phys Med Biol* **58**(6), 1705–23.

O'Brien R T, Cooper B J, Kipritidis J, Shieh C & Keall P J 2014 *Phys Med Biol* **59**(3), 579–95.

O'Brien R T, Cooper B, Shieh C C, Stankovic U, Keall P J & Sonke J 2016 *Phys Med Biol* **61**(9), 3488–99.

O'Brien R T, Kipritidis J, Shieh C C & Keall P J 2014 *Phys Med Biol* **59**(19), 5631–49.

Rit S, Oliva M V, Brousmiche S, Labarbe R, Sarrut D & Sharp G C 2014 *Xvii International Conference on the Use of Computers in Radiation Therapy (Iccr 2013)* **489**.

Ruan D, Fessler J A, Balter J M & Keall P J 2009 *Phys Med Biol* **54**(15), 4777–92.

Shieh C, Kipritidis J, O'Brien R T, Cooper B J, Kuncic Z & Keall P J 2014 *Medical Physics* **41**(4), 041912.

Sonke J J, Zijp L, Remeijer P & van Herk M 2005 *Medical Physics* **32**(4), 1176–1186.

Stankovic U, Ploeger L S, Sonke J J & van Herk M 2016 *Medical Physics* **43**(3), 1057–64.

Taguchi K 2003 *Medical Physics* **30**(4), 640–650.

Yan, H. Wang X, Yin W, Pan T, Ahmad M, Mou X, Cervino L, Jia X & Jiang S B 2013 *Phys Med Biol* **58**(5), 1447–1464.

Yan, H. Zhen X, Folkers M, Li L, Pan T, Cervino L, Jiang S B & Jia X 2014 *Medical Physics* **41**(7), 071903.

Zijp L, Sonke J & Herk M 2004 *International conference on the Use of Computer in Radiation Therapy* pp. 507–509.